JGP Journal of General Physiology

RESEARCH ARTICLE

Singlet oxygen modification abolishes voltage-dependent inactivation of the sea urchin spHCN channel

Vinay Idikuda*, Weihua Gao*, Khade Grant, Zhuocheng Su, Qinglian Liu, and Lei Zhou

Photochemically or metabolically generated singlet oxygen ($^1O_2$) reacts broadly with macromolecules in the cell. Because of its short lifetime and working distance, $^1O_2$ holds potential as an effective and precise nanoscale tool for basic research and clinical practice. Here we investigate the modification of the spHCN channel that results from photochemically and chemically generated $^1O_2$. The spHCN channel shows strong voltage-dependent inactivation in the absence of cAMP. In the presence of photosensitizers, short laser pulses transform the gating properties of spHCN by abolishing inactivation and increasing the macroscopic current amplitude. Alanine replacement of a histidine residue near the activation gate within the channel's pore abolishes key modification effects. Application of a variety of chemicals including $^1O_2$ scavengers and $^1O_2$ generators supports the involvement of $^1O_2$ and excludes other reactive oxygen species. This study provides new understanding about the photodynamic modification of ion channels by $^1O_2$ at the molecular level.

Introduction

Molecular oxygen (O_2) is indispensable for sustaining most forms of life on earth. Molecular oxygen has three electronic configurations: the triplet ground state ($^3\Sigma$) and the first and the second singlet excited states ($^1\Delta$ and $^1\Sigma$; Kochevar, 2004; Ogilby, 2010). Singlet oxygen ($^1O_2$, mainly referring to the $^1\Delta$ state because of its longer lifetime) is highly reactive and oxidizes a wide range of molecules, from pollutants in the water and air to most macromolecules in the cell, including DNA, protein, and unsaturated lipids. Under physiological conditions, $^1O_2$ can be produced either through photochemical processes involving three key elements (photosensitizer, oxygen, and light; DeRosa and Crutchley, 2002) or through metabolic processes involving other reactive oxygen species (ROS) and certain enzymes (Kanofsky et al., 1988; Mano et al., 2014; Onyango, 2016; Prasad et al., 2016). In the cells from the skin and eye, intracellular compounds including flavins and NADH/NADPH are efficient photosensitizers, so $^1O_2$ can be generated under the sunlight (da Silva et al., 2016). This process has been linked to aging and cancer development in these cells, especially after they get excessive exposure to UVA light (320–400 nm; Baier et al., 2006; Bäumler et al., 2012). In liver tissues, $^1O_2$ can be generated in the dark through the oxidation of triplet carbonyls, a biochemical process catalyzed by peroxidase (Mano et al., 2014). Enzymatic generation of $^1O_2$ has also been observed in stimulated neutrophils, macrophages, and plants (Steinbeck et al., 1992; Klotz et al., 2003).

$^1O_2$ is very unstable in aqueous solution, with a lifetime of microseconds and an effective range (working distance) of nanometers. Low levels of $^1O_2$ within the cell may function as an intracellular second messenger by modifying the function of molecules in the vicinity (Klotz et al., 2003; Kochevar, 2004). But high levels of $^1O_2$, especially the $^1O_2$ generated through photochemical reactions, is cytotoxic and has been used as a tool to specifically ablate the function of certain biomolecules and cells. For example, commonly used fluorescent molecules, such as fluorescein (FITC) and certain fluorescent proteins, are effective photosensitizers. In chromophore-assisted light inactivation, fluorophore-tagged antibody recognizes and forms a complex with the target protein (Tour et al., 2003; Wojtovich et al., 2016). Upon light illumination, $^1O_2$ is generated and specifically abolishes the function of the target protein in close vicinity (Liao et al., 1994; Tour et al., 2003; Sack et al., 2013). Similarly, in photodynamic therapy, light is guided to the target tissue to excite the preadministered photosensitizers. Target cells are damaged by $^1O_2$ but are eventually killed through a combination of apoptosis, necrosis, and acutely triggered local immune responses. Photodynamic therapy has been approved by the U.S. Food and Drug Adminis-

Department of Physiology and Biophysics, School of Medicine, Virginia Commonwealth University, Richmond, VA.

*V. Idikuda and W. Gao contributed equally to this paper; Correspondence to Lei Zhou: lzhou@vcu.edu.

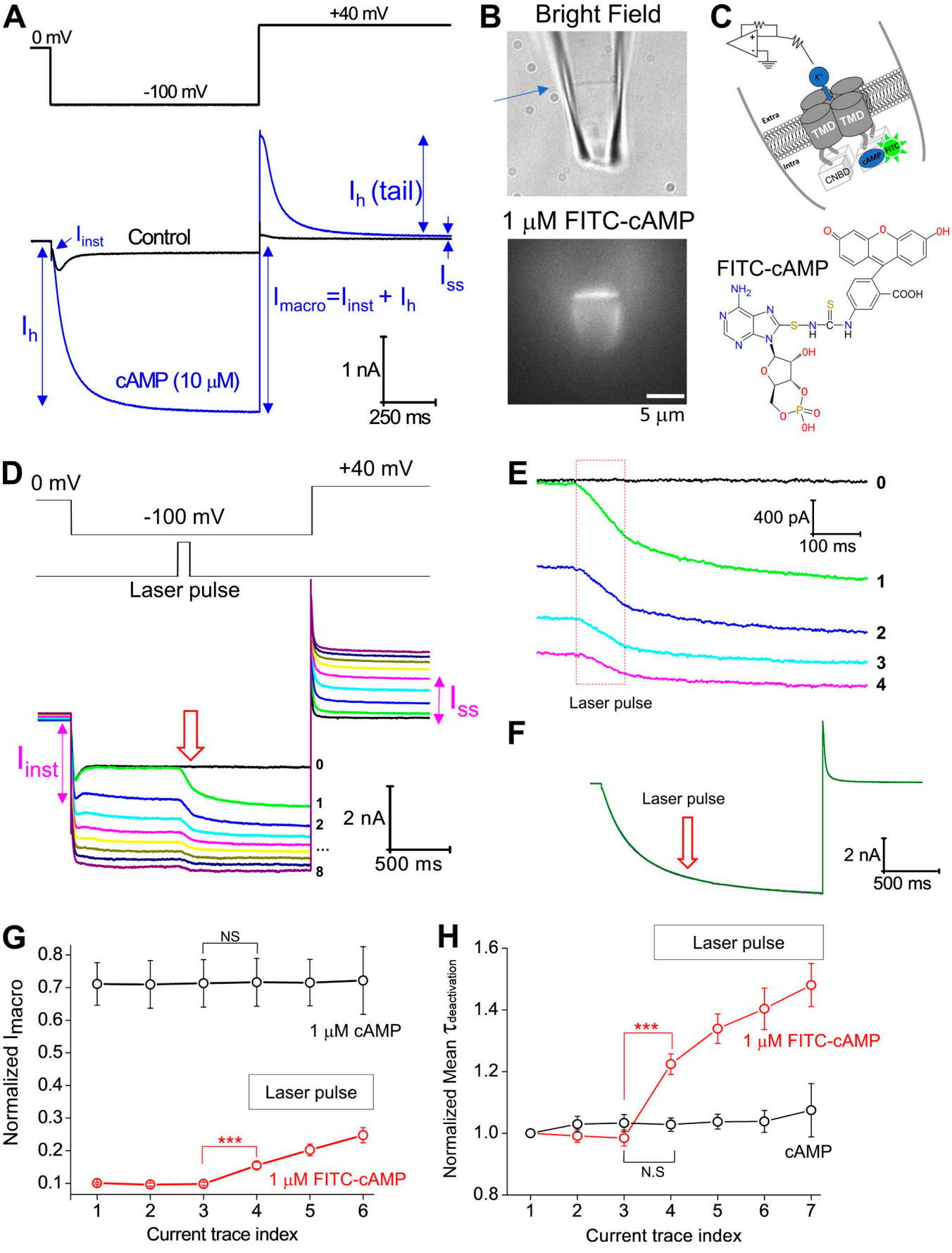

tration to treat cancers of the esophagus, lung, and skin and other diseases related to the skin and eye (Agostinis et al., 2011).

In spite of its broad application potential, little is known about the mechanism of $^1O_2$ modification at the molecular level. $^1O_2$ is not a radical and does not share similar chemical mechanisms with well-studied ROS, including hydrogen peroxide (H_2O_2), superoxide, hydroxyl radical, and nitric oxide (NO; Schweitzer and Schmidt, 2003). The volatile chemical nature of $^1O_2$, the wide range of molecules that react with $^1O_2$, and the heterogeneous distributions of oxygen and photosensitizer together make $^1O_2$ a challenging research target. Previous studies have addressed $^1O_2$ modification of protein molecules including ion channels and transporters (Valenzeno and Tarr, 1991; Eisenman et al., 2007; Babes et al., 2016; Jiang et al., 2017). To produce observable effects, these photodynamic studies often required long light exposure on the timescale of minutes. This is in contrast to the extreme short microsecond lifetime of $^1O_2$. Additionally, these experiments were performed using whole-cell or tissue preparations that contain complex intracellular signaling pathways, thus complicating conclusions at the molecular level. A sensitive and well-defined working system for studying $^1O_2$ has become necessary.

Previously, we had studied $^1O_2$ modification of mouse HCN2 (mHCN2) channel (Gao et al., 2014). HCN channels encode the I_h (or I_f) current that was originally isolated from neurons and cardiac cells (Robinson and Siegelbaum, 2003; Biel et al., 2009). Four mammalian isoforms, HCN1 to HCN4, and an isoform from sea urchin, spHCN, have been cloned and extensively studied (Gauss et al., 1998; Ludwig et al., 1998; Santoro et al., 1998). Each functional HCN channel contains four subunits, with each subunit containing a six-helix transmembrane domain, which is homologous to that of the voltage-gated K channel, and a canonical cyclic nucleotide-binding domain (CNBD) in the C terminus. Thus, HCN channels are equipped with the gating machineries for both voltage- and ligand-dependent gating processes. We have applied the patch-clamp fluorometry (PCF) technique and used different fluorescently labeled cAMP molecules as a marker to study the state-dependent interactions between cAMP and the full-length mHCN2 channel (Wu et al., 2011, 2012).

We have previously shown that laser pulses applied to the mHCN2 channel in complex with the cAMP analogue FITC-cAMP slow down the channel deactivation and increase the voltage-insensitive, instantaneous (I_{inst}) component (Proenza et al., 2002; Gao et al., 2014). The I_{inst} carried by the HCN channel refers to the current component that shows an immediate response to a change in the membrane potential but without much of the time-dependence typically observed with voltage-dependent gating (Fig. 1 A). Because of its insensitivity to voltage, the I_{inst} should be constitutively conductive regardless of the membrane potential. In both native and heterologous expression systems, the I_{inst} carried by HCN channels has been detected, but the corresponding molecular basis underlying the decoupling between the gate and the voltage sensor has been unclear (Macri and Accili, 2004; Mistrík et al., 2006; Proenza and Yellen, 2006). The photodynamic modification of mHCN2 channels was actually an effective approach for generating I_{inst}.

The study on the photodynamic modification of mHCN2 channels led us eventually to the identification of $^1O_2$ as the major player. Here we extend the investigation from mHCN2 to spHCN channel, which shows strong voltage-dependent inactivation in the absence of cAMP, a unique feature that differentiates it from the mammalian isoforms. cAMP binding removes the inactivation in spHCN channel so that it behaves similarly to HCN1 and HCN2 channels. We found that $^1O_2$ modification removes the voltage-dependent inactivation of the spHCN channel in the absence of cAMP. The photodynamic modification is state dependent and exerts different effects on closed versus inactivated spHCN channels. Finally, we investigated several chemical processes to help establish $^1O_2$ as the major player in this process.

Materials and methods

Functional expression in *Xenopus laevis* oocytes and electrophysiological characterization

The cDNA sequence encoding spHCN was provided by Dr. R. Seifert and Dr. U.B. Kaupp from the Center of Advanced European Studies and Research (Caesar, Bonn, Germany; Gauss et al., 1998). The spHCN cDNA was inserted into the pGEM-HE vector for expression in *Xenopus* oocytes (Liman and Buck, 1994). mMessage machine (Ambion) was used for cRNA synthesis. 25–30 ng cRNA encoding the spHCN channel was injected into each oocyte at stage VI. For patch-clamp recording, the electrode solution (extracellular) and bath solution (intracellular) were symmetrical and contained 110 KCl, 2 NaCl, 10 HEPES, and 1 EDTA (all in mM; pH 7.4 adjusted by KOH). A Model 2400 patch clamp amplifier (A-M Systems) was used in all voltage-clamp recordings. Current

Figure 1. **Photodynamic modification of the spHCN channel in complex with FITC-cAMP. (A)** Top: Voltage protocol for channel activation (−100 mV) and tail current recording (+40 mV). Bottom: WT spHCN channels show strong voltage-dependent inactivation in the absence of cAMP (black). With cAMP, the spHCN channel opens without any obvious inactivation (blue). The definitions of I_{inst}, I_h, I_{macro}, I_h(tail), and I_{ss} are illustrated. Background leak conductance was not subtracted. **(B)** Top: Bright-field image of a piece of membrane patch (indicated by an arrow) held within the glass recording pipette. Bottom: Fluorescence image of the spHCN channel in complex with 1 µM 8-FITC-cAMP. Membrane patches from uninjected oocytes (no channel expressed) only show fluorescence intensity at background level (not shown). **(C)** Top: Schematic drawing of the patch-clamp recording under the inside-out configuration. Bottom: Chemical structure of 8-FITC-cAMP. **(D)** Top: Voltage step protocol and the timing of laser pulse. Bottom: The last current trace before (black; trace 0) and after (with color; traces 1–8) laser pulse application. Numbers from 1 to 8 represent the order of applied laser pulses and the corresponding current traces. The prominent increases in I_{inst} after the third laser pulse and in I_{ss} after the fourth laser pulse are labeled (magenta). **(E)** A zoomed view over the moment when laser pulses were applied. Red box in dashed lines represents the laser pulses with 100-ms duration. **(F)** Laser pulses have no obvious effects on the spHCN channel in complex with regular 1 µM cAMP. **(G)** Averaged results (n = 13) showing the effect of laser pulse on the amplitude of I_{macro}. The horizontal box (with laser pulse labeled) indicates the current episodes with laser pulse treatment. Current amplitudes were normalized to the maximal value measured in the presence of 10 µM cAMP before the application of laser pulses. **(H)** Averaged results (n = 13) showing the effect of laser pulses on the time constant of deactivation. ***, $P \le 0.001$. Error bars represent SEM.

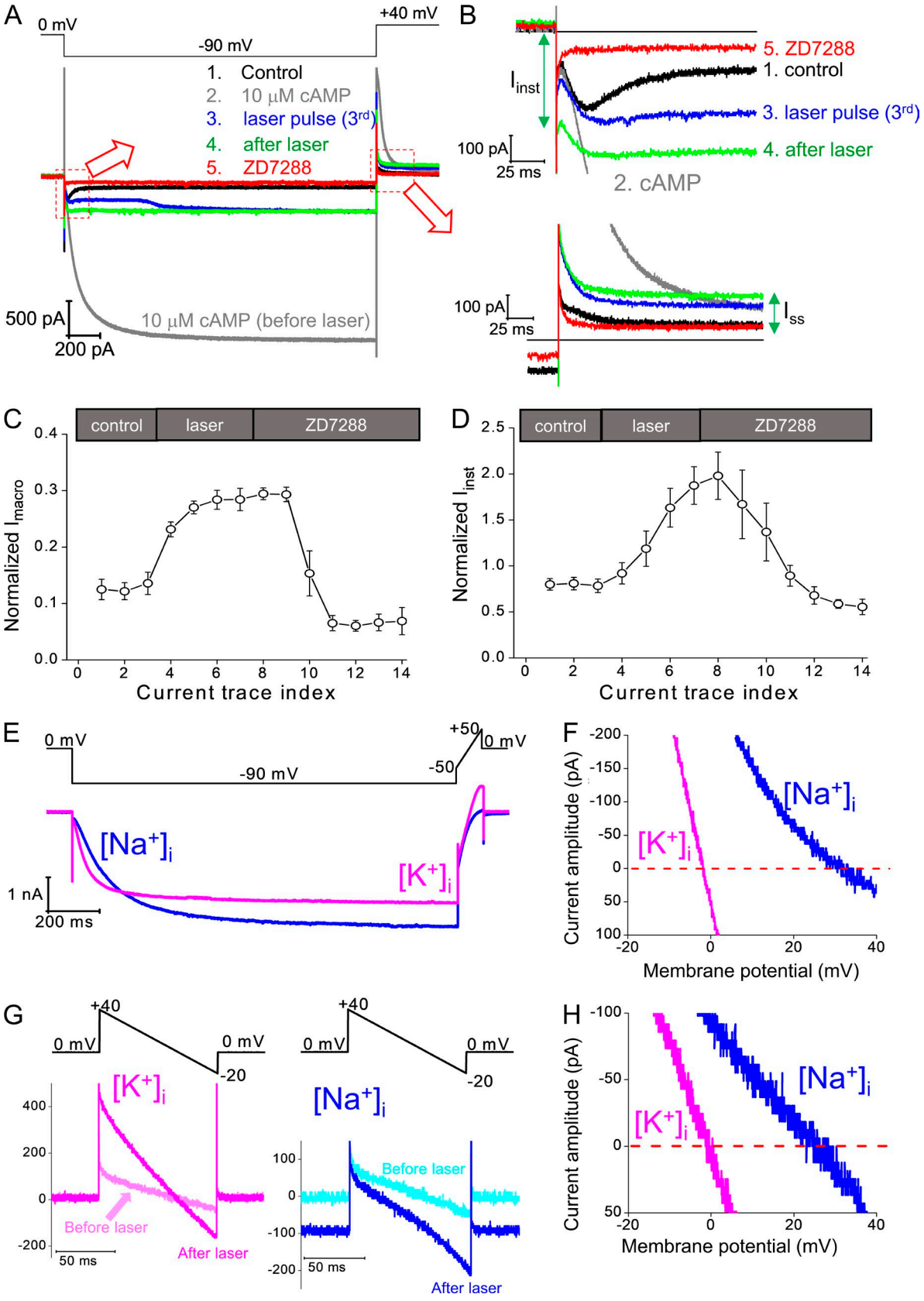

Figure 2. **I_h and I_{inst} share similar sensitivity to ZD7288, an HCN channel–specific blocker, and K^+/Na^+ selectivity. (A)** Top: Voltage protocol. Bottom: Four current traces in sequence showing control (no cAMP), 10 μM cAMP, the third trace with laser pulse (with 1 μM FITC-cAMP), after laser pulses stopped and washing off FITC-cAMP, and ZD7288 (100 μM). **(B)** Zoomed views showing the I_{inst} (top) and the I_h(tail) and I_{ss} (bottom). **(C)** Averaged results showing that laser pulses applied in the presence of FTIC-cAMP increase the amplitude of I_{macro}, which can be blocked by ZD7288. **(D)** Averaged results showing that laser pulses

signals were filtered at 5 kHz and digitized by Digidata 1320A (Axon Instruments) at 10 kHz. The WinWCP program (University of Strathclyde, Glasgow) was used for data acquisition. All experiments were performed at room temperature.

For the voltage-dependent channel activation curve shown in Fig. 4 B, the Boltzmann equation was used to fit the normalized I_h(tail) amplitudes:

$$Normalized\ I_h = A2 + \frac{A1 - A2}{1 + exp^{\frac{V - V_{1/2}}{slope}}},$$

where *A*1 and *A*2 represent the peak and the offset values, respectively.

Here we used a single-exponential function to obtain an estimation of the deactivation kinetics mainly for comparison purposes. It is known that the activation and deactivation of the HCN channels involves complex subunit–subunit coordination and does not follow a simple single-exponential (mono-exponential) kinetics. A double-exponential function will give a better fit, but because of a lack of physical meaning, it is not popularly used in the literature. The portion of the deactivation current trace is individually selected by putting the first cursor after the capacitance artifact and the second cursor when the current has reached a steady state (for examples, see Fig. S14).

For the measurement of K^+/Na^+ selectivity, K^+ ions in the bath solution (in contact with the intracellular side of the membrane) were replaced by Na^+. Na^+ in the pipette solution was also replaced by K^+. We used the following equation to calculate the ratio of K^+/Na^+ selectivity:

$$\frac{P_K}{P_{Na}} = \frac{[Na]_o - exp^{\frac{REV}{RT/F}} \cdot [Na]_i}{exp^{\frac{REV}{RT/F}} \cdot [K]_i - [K]_o},$$

where *REV* is the reversal potential. $[K]_i$ and $[Na]_o$ are both zero.

PCF

The PCF setup was assembled based on an Olympus IX71 microscope equipped with a 100× oil lens (Olympus, Plan N 100×, NA 1.25). A 473-nm diode-pumped solid-state laser (Ultralasers) was used as the excitation light source. The following filter settings were used for recording FITC fluorescence signal: exciter, D480/30; dichroic mirror, DC505LP; and emitter, D510LP (Chroma Technology). Optical signals were detected by a 16-bit electron multiplying charge-coupled device (EMCCD) camera (Cascade 1K; Photometrics). The laser light source, the charge-coupled device (CCD) camera exposure, and the amplifier for patch-clamp recording were synchronized by transistor–transistor logic signals. As confirmed by histogram of the intensities of all pixels, the optical signals were collected within the linear range of the CCD camera. ImageJ (National Institutes of Health) was used to analyze the fluorescence images (Schneider et al., 2012).

For routine quantification of the intensity profile of the excitation light, a fluorescent plate (Chroma Technology Corp.) was mounted at the focal plane of the objective lens (Fig. S1, A and B). The fluorescence image of the plate was recorded with the same optical configuration (473-nm laser, filter sets and dichroic mirror, EMCCD camera). Exposure time and gain of the camera were reduced to prevent saturation (65,535 for a 16-bit camera). The peak area of the excitation light was marked on the computer monitor to help position the membrane patch held within the glass pipette (Fig. S1 C). The membrane patch was positioned to the center of the excitation light.

An optical power meter (Model 835; Newport) was used to measure the total light output of the objective lens (100× oil), which was ∼20 µW. Based on the profile of the fluorescence intensity of the whole image, the light intensity near the tip of the glass pipette within a 10 × 10–µm^2 square was ∼1,036 mW/cm^2 or 10,360 W/m^2. The diameter of the pipette was ∼10 µm, and the resistance was ∼0.8 MΩ. The glass type was KIMAX-51.

Chemicals

All chemicals were purchased from Sigma-Aldrich or Fisher Scientific unless otherwise noted. 8-FITC-cAMP (Fig. 1 B) was purchased from Biolog.de (catalog no. F002). The stock solution (1 mM) was made by adding 1 ml ddH_2O to the vial containing 1 µmol 8-FITC-cAMP. The stock solution of Rose Bengal (1 mM) was made by adding ddH_2O and stored as aliquots at −20°C. The stock solution was protected from light and diluted in the bath solution just before the experiments. Hydrogen peroxide was diluted in the bath solution to a final concentration of 10 mM just before experiments. Sodium hypochlorite was diluted directly in the bath solution to obtain a final concentration of 10 mM. Both hydrogen peroxide and hypochlorite had to be freshly prepared just before experiments. Stock solution of xanthine was made in 1 M NaOH and then diluted to 5 mM in bath solution. 15 mU of xanthine oxidase in bath solution was added through a separate perfusion line. Hydroxyl radical was generated by mixing 1 mM $FeSO_4$ with 15 mM hydrogen peroxide, which were also delivered to the recording chamber through separate perfusion lines. Stock solution of $FeSO_4$ was prepared in ddH_2O.

The experimental configuration for solution mixing is shown in Fig. S12 A. In brief, the solutions containing H_2O_2 and ClO^- were delivered through a double-barrel glass pipette. The tip of the glass pipette was positioned at a distance from the double-barrel

applied in the presence of FTIC-cAMP increase the amplitude of I_{inst}, which can also be blocked by ZD7288. Error bars represent SEM. **(E)** Top: Voltage protocol for I_h activation (0 to −90 mV) and a voltage ramp (−50 to 50 mV) used for the measurement of reversal potential before light pulses. Bottom: Current traces recording from the same membrane patch with symmetrical $[K^+]_{in}/[K^+]_{out}$ (magenta) or $[Na^+]_{in}/[K^+]_{out}$ (blue). 10 µM cAMP was added to the bath solution on the intracellular side. **(F)** Cross-plot of current amplitude versus membrane potential during the voltage ramp for I_h. Averaged results: 1.3 ± 0.3 mV (K^+_i); −27.8 ± 1.2 mV (Na^+_i); *n* = 4. **(G)** Top: A voltage ramp (+40 to −20 mV) was used for the measurement of reversal potential of I_{inst}. Bottom: Current traces recorded from the same membrane patch with symmetrical $[K^+]_{in}/[K^+]_{out}$ (magenta, left) or $[Na^+]_{in}/[K^+]_{out}$ (blue, right). Current traces in light colors are recorded before laser pulses and mainly caused by nonspecific leak conductance. Current traces in dark colors are recorded after laser pulses stopped and in the absence of FITC-cAMP. **(H)** Cross-plot of current amplitude versus membrane potential during the voltage ramp for the I_{inst} after laser pulses. Averaged results: 0.9 ± 0.2 mV (K^+_i); −26.5 ± 0.9 mV (Na^+_i); *n* = 4.

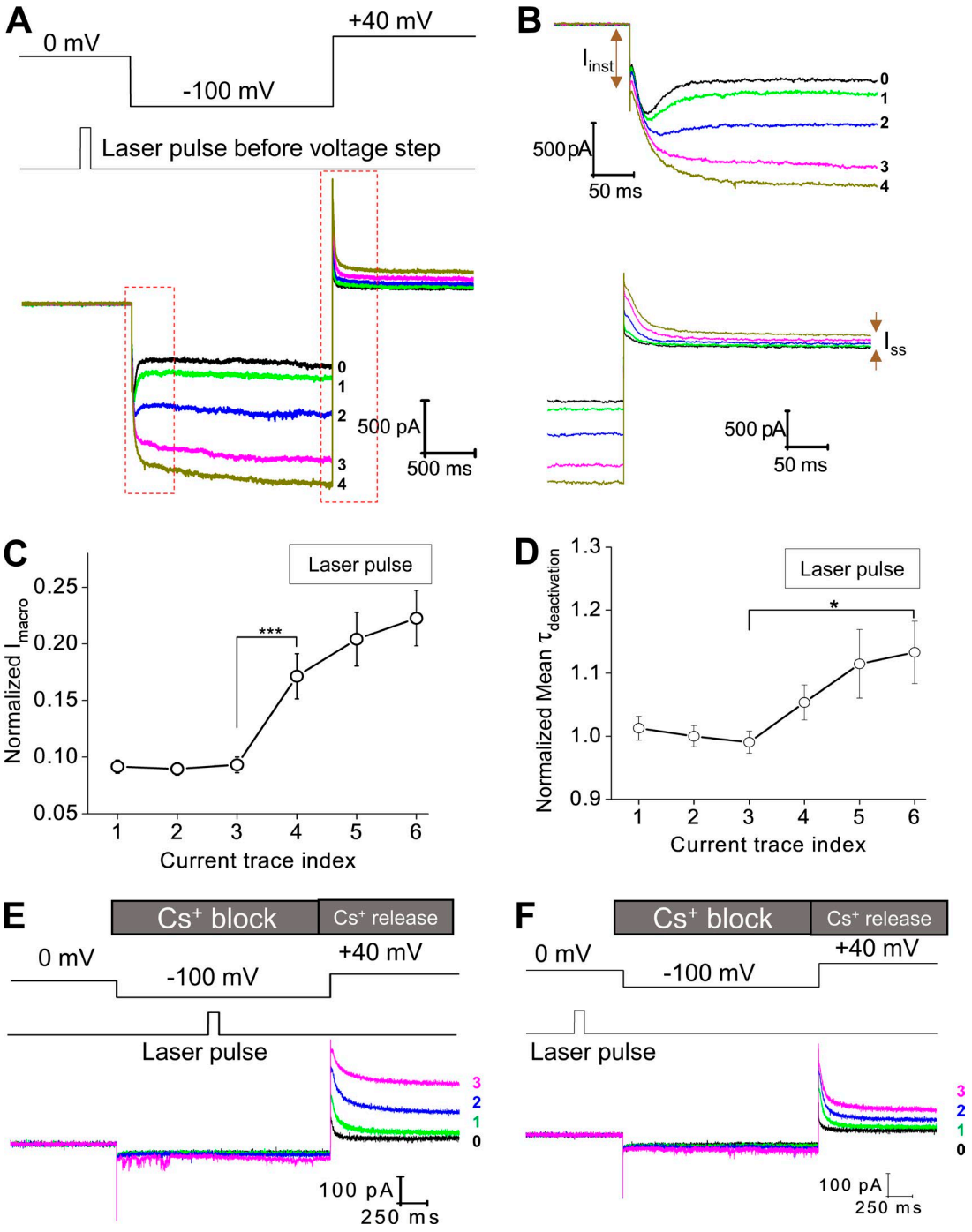

Figure 3. **Photodynamic modification of the spHCN channel in the closed state and the sensitivity of modified spHCN channels to Cs^+. (A)** Top: Voltage command and the timing of laser pulses. Laser pulses were applied preceding the hyperpolarization voltage step when most of the channels should stay in the closed state. Bottom: Current traces recorded with 1 µM FITC-cAMP in the bath solution. The last control trace before laser pulse is shown in black and labeled 0. **(B)** Zoomed views of the region within the red box shown in A. **(C)** Averaged (n = 15) results showing the effect of laser pulses on the amplitude of macroscopic current. ***, P ≤ 0.001. **(D)** Averaged (n = 15) results showing the effect of laser pulses on the time constant of deactivation. *, P ≤ 0.05. Error bars represent SEM. **(E)** During the −100-mV voltage step, Cs^+ applied to the extracellular side of the membrane blocks the spHCN current after photodynamic modification (laser pulse during voltage step). The following depolarizing voltage step from −100 to +40 mV released the block by Cs^+ and revealed the effects of photodynamic modification. Photodynamic modification leads to slowdown in channel deactivation and increases in I_h(tail) and I_{ss}. Black, last current trace before laser pulse. Green, traces with laser pulses. **(F)** Laser pulses were applied preceding the hyperpolarization voltage step. Cs^+ blocks the macroscopic current at −100 mV. The voltage step from −100 to +40 mV released the Cs^+ block and revealed the effects of photodynamic modification. Detailed analyses are shown in Fig. S5.

as indicated. For the adjustment in the Z dimension, the lower edge of the double barrel and the pipette tip were adjusted to the same focal plane.

Related chemicals

Other chemicals were as follows: Rose Bengal (R323-25; Fisher Scientific); H_2O_2 (BP2633; Fisher Scientific); Iron (II) sulfate

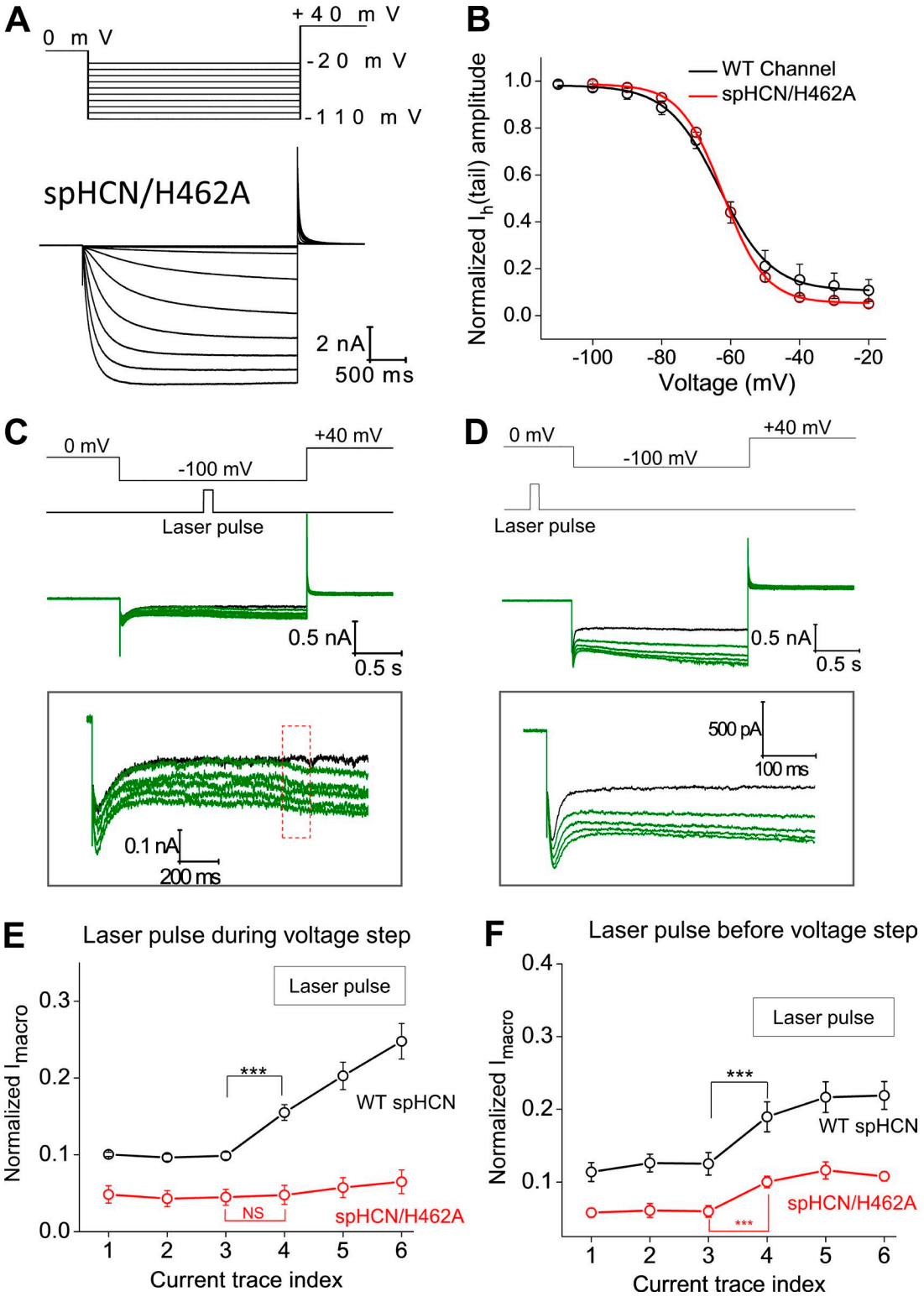

Figure 4. **spHCN/H462A mutant channel shows minimal responses to photodynamic modification. (A)** Top: Voltage steps used for channel activation and tail current recording. Bottom: Current traces of the spHCN/H462A mutant channel recorded in the presence of 10 µM cAMP. **(B)** Averaged voltage-dependent activation curve of the WT (black, n = 5; $V_{1/2}$, −63.2 ± 0.8 mV) and spHCN/H462A mutant (red, n = 6; $V_{1/2}$, −62.2 ± 0.8 mV) channels. **(C)** The spHCN/H462A mutant channel shows minimal responses to laser pulses during the voltage step from 0 to −100 mV. A zoomed view of the current trace is shown below. **(D)** Laser pulses applied before the voltage step leads to small increases in macroscopic current but minimal effects on channel inactivation. A zoomed view of the current trace is shown below. **(E)** Averaged results showing the effect of laser pulses (applied during voltage step) on the I_{macro} amplitude of the WT (n = 13, black) and spHCN/H462A mutant (n = 5, red) channels. ***, P ≤ 0.001. **(F)** Averaged results showing the effect of laser pulses (applied before voltage step) on the I_{macro} amplitude of the WT (n = 15, black) and spHCN/H462A mutant (n = 5, red) channels. ***, P ≤ 0.001. Error bars represent SEM.

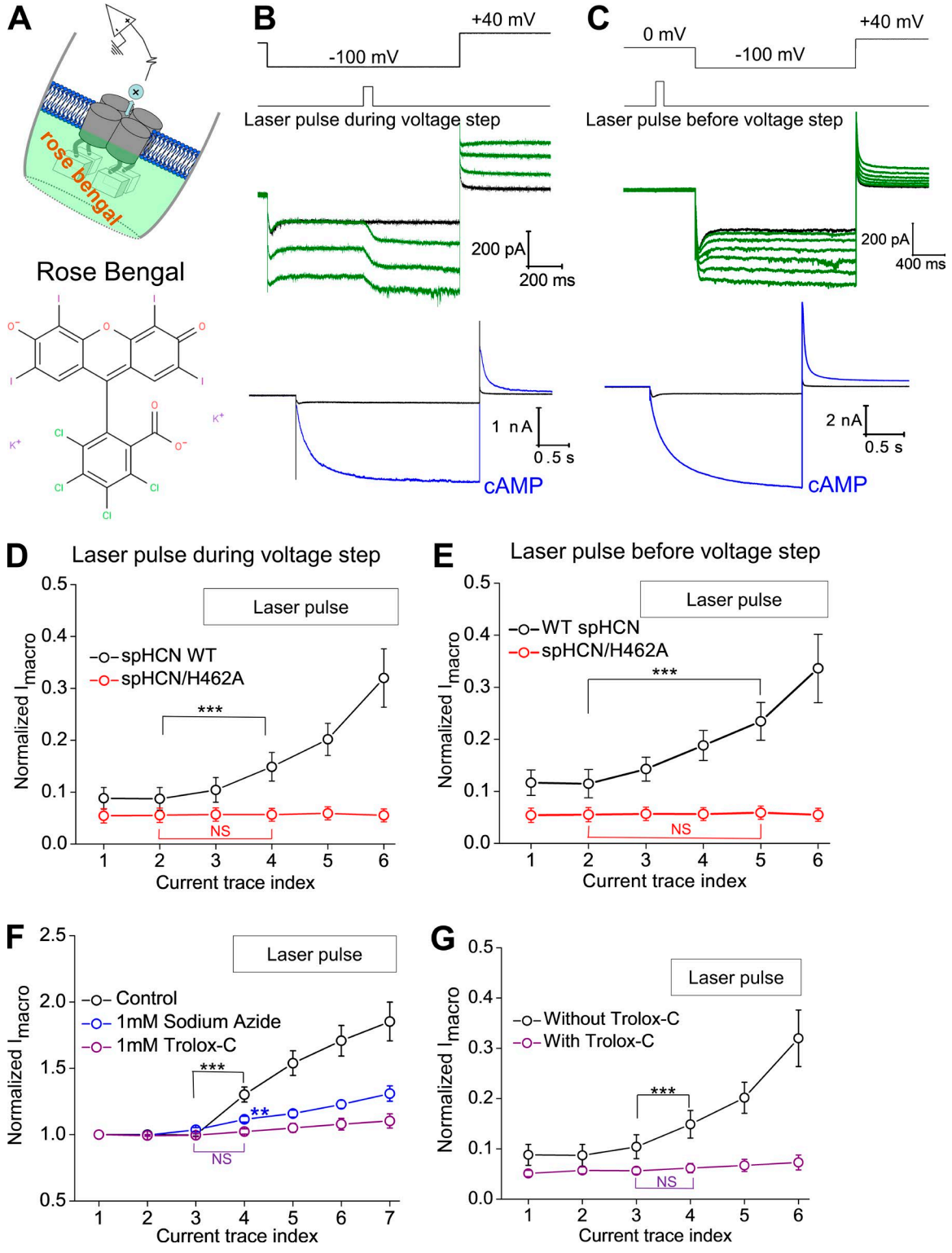

Figure 5. **Applications of a popularly used photosensitizer, Rose Bengal, and $^1O_2$ quenchers (sodium azide and Trolox-C) support the involvement of $^1O_2$. (A)** Schematic drawing of the experiment configuration. Rose Bengal was applied to the bath solution and in contact with the intracellular side of the channel. **(B)** In the presence of 100 nM Rose Bengal, laser pulses were applied in the middle of the voltage step from 0 to −100 mV. The current traces recorded before the application of laser pulses are shown below. **(C)** In the presence of 100 nM Rose Bengal, laser pulses were applied preceding the voltage step to −100 mV. The current traces recorded before the application of laser pulses are shown below. **(D)** Averaged results showing the effect of laser pulses (during the voltage step) on the I_{macro} amplitude of the WT (n = 8, black) and spHCN/H462A mutant (n = 8, red) channels. **(E)** Averaged results showing the effect of laser pulses (before the voltage step) on the I_{macro} amplitude of the WT (n = 5, black) and spHCN/H462A mutant (n = 5, red) channels. **(F)** Averaged

heptahydrate (423731000; Acros Organics); sodium hypochlorite (3336936; Alga Aesar); potassium superoxide (AC325501000; Acros Organics); xanthine (A1107714; Alfa Aesar); and xanthine oxidase (68215110U; EMD Millipore).

Statistics

All statistical tests were performed using the OriginPro program. Error bars in the graphs represent the amplitude of one SEM. Data are presented as mean ± SEM. Student's *t* test was used to evaluate the statistical significance of the results of two independently collected pools of data (unpaired; for example, cAMP vs. FITC-cAMP) or a group of data before and after certain treatments (paired; for example, before and after laser pulses). $P > 0.05$ was considered statistically nonsignificant; *, $P \le 0.05$; **, $P \le 0.01$; ***, $P \le 0.001$.

Online supplemental material

Fig. S1 shows the intensity profile of the excitation light and alignment of membrane patches. Fig. S2 shows effects of photodynamic modification on cell membrane without spHCN channel and illustration of I_{inst}, I_h, I_h (tail), and I_{ss} after photodynamic modification. Fig. S3 shows that the I_{inst} and I_{ss} after photodynamic modification can be up-regulated by cAMP and blocked by ZD7288. Fig. S4 shows that laser pulses applied before and in the middle of the hyperpolarizing voltage step have different impacts on I_{inst} and I_h (tail). Fig. S5 shows that Cs^+ blocks I_{inst} and I_h after photodynamic modification. Fig. S6 shows that WT spHCN channel is more sensitive to photodynamic modification than spHCN/H462A mutant channel. Fig. S7 shows Rose Bengal–mediated photodynamic modification of WT spHCN and spHCN/H472A mutant channels. Fig. S8 shows effects of singlet oxygen quencher Trolox-C on the photodynamic modification of inactivated spHCN channels mediated by Rose Bengal. Fig. S9 shows effects of Trolox-C on the photodynamic modification of closed spHCN channels mediated by Rose Bengal. Fig. S10 shows that Rose Bengal with laser pulses has no effects on empty membrane patch without spHCN channel. Fig. S11 shows that WT spHCN and spHCN/H462A mutant channels show comparable binding of FITC-cAMP. Fig. S12 shows the configuration of the perfusion system for H_2O_2 and ClO^- and averaged results for effects of hydroxyl and superoxide radicals. Fig. S13 shows raw data for the effects of laser pulses during voltage step on amplitudes of I_{macro}. Fig. S14 shows examples of single exponential fitting of deactivating tail current.

Results

Laser pulses abolish the voltage-dependent inactivation of the spHCN channel

We used the inside-out configuration of the patch-clamp technique to record currents from spHCN channels expressed in *Xenopus* oocytes. Unlike mammalian HCN isoforms, spHCN undergoes significant voltage-dependent inactivation. Inactivation of spHCN can be removed by addition of cAMP to the bath solution with a half-maximal effective concentration (EC_{50}) of 0.74 µM (Gauss et al., 1998; Fig. 1 A). The currents showed a voltage-independent instantaneous component, I_{inst}, and a steady-state current after deactivation, I_{ss}. The total or macroscopic current at the end of the hyperpolarizing voltage pulse, I_{macro}, is simply the sum of I_{inst} + I_h (see labels in Fig. 1 A).

Using patch-clamp fluorometry, we found that the fluorescent cAMP analogue 8-FITC-cAMP bound to spHCN (Fig. 1, B and C) but has a less significant effect on channel gating compared with cAMP (Fig. S11 C), most likely because of the bulky and charged FITC group. In the presence of 1 µM 8-FITC-cAMP, spHCN channels showed strong voltage-dependent inactivation (trace 0 in Fig. 1 D; the last trace before laser pulses). With 8-FITC-cAMP in the bath solution, we found that short laser pulses (100 ms) applied to the membrane patch triggered a time-dependent increase in current amplitude (green and other color traces; Fig. 1 D). The laser pulses were applied in the middle of the 2-s-long hyperpolarizing-voltage step when most of the channels were in the inactivated state. As shown in the zoomed view during the 100-ms laser pulse (Fig. 1 E; within the dashed red box), increases in the microscopic (I_{macro}) current were observed. After the laser pulse, the I_{macro} amplitude continued to increase, indicating a continuing shift of the equilibrium from the closed or inactivated state to the open state. The FITC moiety was required for the photodynamic transformation process because the same laser pulse applied to the spHCN channel in complex with cAMP did not increase current (Fig. 1, F and G). In addition, light-activated current was not observed in patches from cells that contained no spHCN channel but were exposed to FITC-cAMP, indicating that spHCN was required (Fig. S2 A).

As previously demonstrated with the mHCN2 channels (Gao et al., 2014), laser pulses significantly prolonged the time constant for deactivation of spHCN (Fig. 1 H). After photodynamic modification, the $\tau_{deactivation}$ was still less than 100 ms, much shorter than the interval between two adjacent current episodes (15 s). Thus, the slowdown in deactivation did not contribute to the increases in the voltage-insensitive current component (I_{inst}; see labels on Figs. 1 D and S2 B). The effects of photodynamic modification were long lasting: they could still be seen 5 min after the end of laser pulses and the washing off of FITC-cAMP (Fig. S3 A). There was noticeable variability from patch to patch in terms of the extent of photodynamic modification of channel inactivation removal and the fraction of I_{inst} within I_{macro}. The geometry and position of membrane patch and the attachment of intracellular particles to the membrane are factors affecting the efficiency of the photodynamic modification (Fig. S13).

Both I_{inst} (measured at −100 mV) and I_{ss} (+40 mV) are conducted by spHCN channel

Similar to previous study on mHCN2 channels, laser pulses led to an increase in spHCN I_{ss}, measured after the completion of

results showing the effect of sodium azide (n = 7, blue) and Trolox-C (n = 8, purple) on the photodynamic modification of WT spHCN channels. FITC-cAMP was the photosensitizer. **(G)** Averaged results showing the effect of Trolox-C (purple) on the photodynamic modification (n = 11) of WT spHCN mutant (n = 7, red) channels. Rose Bengal was the photosensitizer. For D–G, results are mean ± SEM; ***, $P \le 0.001$. Error bars represent SEM.

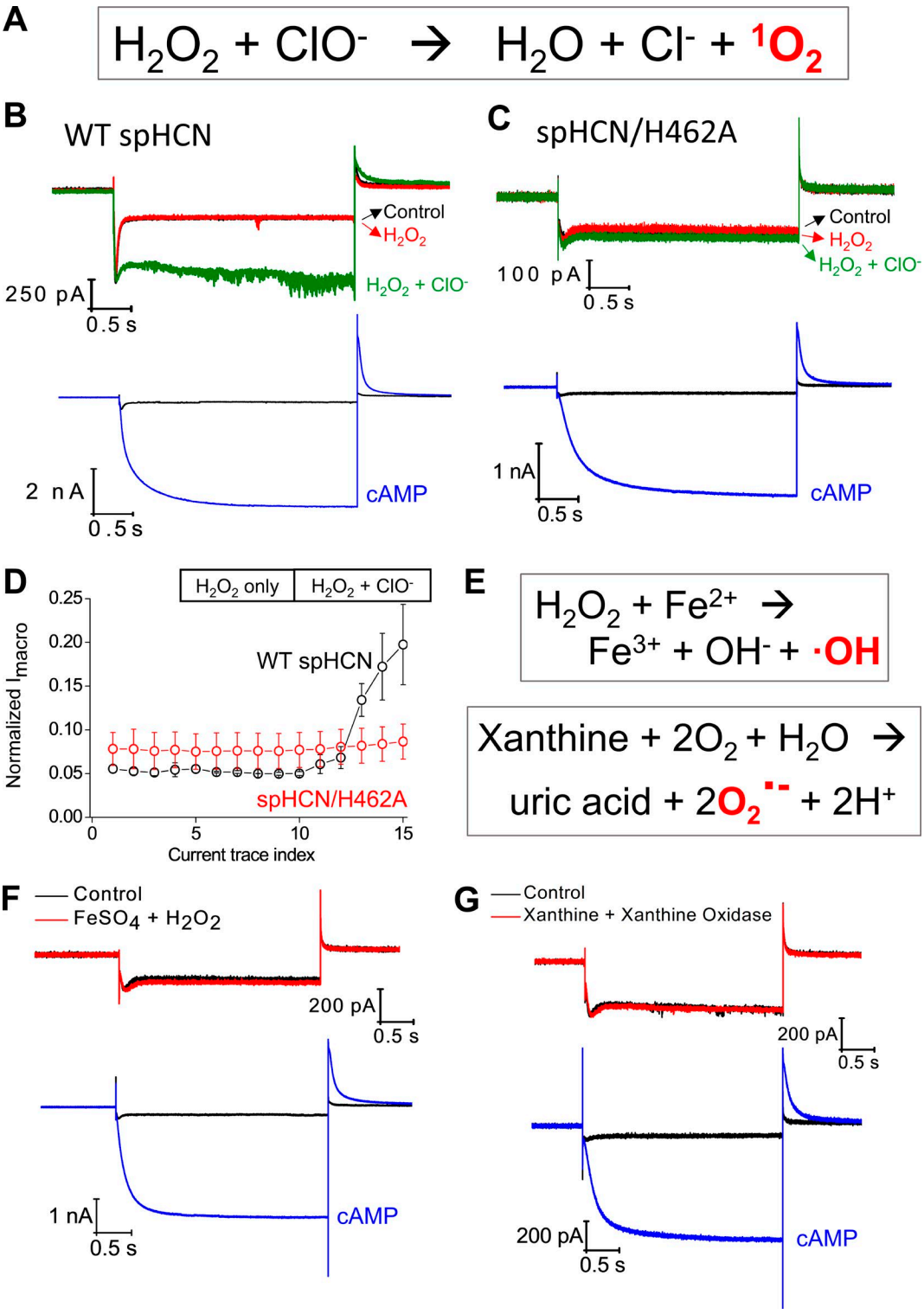

Figure 6. **The function of WT spHCN channel can be modulated by chemically generated $^1O_2$ but not by hydroxyl or superoxide radicals. (A)** Chemical generation of $^1O_2$ by mixing hydrogen peroxide and sodium hypochlorite. **(B)** Top: Current traces of WT spHCN channel recorded under control condition (black), in the presence of 10 mM H_2O_2 only (red), or in the presence of a mixture of 10 mM H_2O_2 and 10 mM NaClO (green). Bottom: Current traces recorded before chemical applications. **(C)** The spHCN/H462A mutant channel shows no responses to the chemical mixture of H_2O_2 and NaClO. Bottom: Current traces recorded before chemical applications. **(D)** Averaged results showing the responses to H_2O_2 or H_2O_2+NaClO by WT (n = 3, black) and H462A mutant (n = 3, red) spHCN channels. Error bars represent SEM. **(E)** Reaction schemes of the chemical generation of hydroxyl or superoxide radicals. **(F)** The WT spHCN channel shows no response to the mixture of $FeSO_4$ (1 mM) and H_2O_2 (15 mM; n = 5). Bottom: Current traces recorded before application of chemicals. **(G)** The WT spHCN channel shows no response to the mixture of xanthine (5 mM) and xanthine oxidase (15 mU; 6 min of incubation; n = 6). Bottom: Current traces recorded before chemical applications.

deactivation of I_h (tail) at +40 mV (Fig. 2, A and B). Because the light-activated spHCN current is long lasting, it can also be measured as I_{inst} in the following current trace, at the very beginning of the voltage jump from 0 to −100 mV. Importantly, the amplitudes of I_{ss} (+40 mV; present trace) and the I_{inst} (−100 mV) of the subsequent trace are tightly correlated (Fig. S3 B).

To confirm that the increased I_{inst} and I_{ss} are conducted by spHCN channels, we applied ZD7288, an HCN channel–specific blocker (BoSmith et al., 1993), to the intracellular side (bath solution). In chronological order, the current traces in Fig. 2 (A and B) correspond to control trace before the laser pulse and cAMP (black; 1), maximal current in 10 µM cAMP (gray; 2), current trace with the third laser pulse (blue; 3), current trace after the end of the laser pulse (green; 4), and current trace in the presence of ZD7288 (red; 5). The difference between the green trace after photodynamic modification and the red trace with ZD7288 demonstrates the block of the light-induced component of I_{inst}, I_h, I_h (tail), and I_{ss} and supports that the light-induced increase in current were caused by spHCN. Averaged results are shown in Fig. 2 (C and D). Moreover, both I_{inst} and I_{ss} were increased by cAMP applied to the bath solution (after the stop of laser pulses; Fig. S3 A), further supporting that the light-induced increases in I_{inst} and I_{ss} were caused by spHCN channel.

To further test whether the I_{inst} is carried by the spHCN channels, we measured the K^+/Na^+ selectivity of I_{inst}. HCN channels are weakly selective for K^+, with P_K/P_{Na} between 3 and 4. We first measured the P_K/P_{Na} of the maximal current before laser pulses (in the presence of cAMP; Fig. 2 E). With the K^+ solution in the pipette (extracellular), we measured currents with K^+ in the bath solution (intracellular) and then replaced K^+ in the bath with Na^+ to determine any changes in reversal potentials. The shift in the reversal potential of the I_h current from 1.3 ± 0.3 mV ($[K^+]_i$) to −27.8 ± 1.2 mV ($[Na^+]_i$; n = 4) confirmed the weak selectivity for K^+ over Na^+ by spHCN channels (Fig. 2 F). Then we measured P_K/P_{Na} using a voltage ramp from +40 mV to −20 mV, which was chosen to minimize I_h activation (Fig. 2 G, top). The current traces recorded before laser pulse (light magenta and light cyan in Fig. 2 G, bottom) should correspond mostly to nonspecific conductance, since both the reversal potentials and the holding current at 0 mV were close to zero with $[Na^+]_i$ solution. After laser pulse treatment, there was a significant increase in current amplitude, and the reversal potential was shifted from 0.9 ± 0.2 mV ($[K^{++}]_i$) to −26.5 ± 0.9 mV ($[Na^+]_i$; n = 4). Therefore, the similar P_K/P_{Na} between I_h and I_{inst} provides additional evidence that after photodynamic modification I_{inst} was mainly carried by spHCN channels.

Photodynamic modification of the spHCN channel in the closed state

In the above experiments, laser pulses were applied in the middle of the hyperpolarizing voltage step, when most of the channels were in the inactivated state. Laser pulses directly initiated a time-dependent channel opening process. Next, we studied the effects of laser pulses on the channel in the closed state by applying laser pulses preceding the hyperpolarizing voltage step when most of the channels were in the closed state (Fig. 3 A). In the presence of 1 µM FITC-cAMP, laser pulses (100 ms) did not lead to immediate channel opening; however, in response to the following hyperpolarization voltage step, channel inactivation became less prominent (Fig. 3 B, top). Correspondingly, the amplitude of I_{macro} and the I_h component increased (Fig. 3 B [bottom], C, and D). Laser pulses applied to closed channels led to moderate increases in I_{inst} and I_{ss}. Interestingly, different from the laser pulses applied during the voltage step to mainly inactivated channel, laser pulses applied to closed spHCN channels resulted in more pronounced increases in I_h but only small increases in I_{inst} (Fig. S4).

To confirm whether the above changes in ionic current were indeed carried by the spHCN channel on the membrane, we added 100 µM ZD7288 to the bath solution or 2 mM Cs^+ to the pipette solution. Similar to the results of laser pulse during voltage step, ZD7288 blocked the increases in I_{macro} and I_{inst} upon photodynamic modification with laser pulse before voltage steps (Fig. S3, C–E). Cs^+ applied to the extracellular side can effectively block the inward HCN current in a voltage-dependent manner (Fain et al., 1978; Barnes and Hille, 1989). Indeed, we observed a complete block of ionic current by Cs^+ during the −100-mV voltage step after laser pulses, which excludes significant contributions by nonspecific leak conductance to the increase in I_{inst} after photodynamic modification (Fig. 3, E and F). To confirm that the channels were photodynamically modified, we monitored the current trace in response to the depolarizing voltage step from −100 to +40 mV, which removes Cs^+ block. The significant increase in I_h(tail) and the nondeactivating I_{ss} confirmed the impacts of the photodynamic modification. Averaged results for the application of Cs^+ are shown in Fig. S5.

A single point mutation, H462A, abolishes effects of photodynamic modification

Among the 20 amino acids, histidine is believed to be the major target of $^1O_2$ (Matheson et al., 1975). Previously, we identified a histidine residue critical to photodynamic modification in the mHCN2 channel, H434, which is located in the last transmembrane domain (S6) and close to the activation gate of HCN channels (Wu et al., 2012). Alanine replacement of H434 abolishes most effects of photodynamic modification on mHCN2 channels. In spHCN channels, the corresponding residue is H462. We started from a basic characterization of the spHCN/H462A mutant channel. The mutant channel behaves similarly to the WT channel, including the binding of FITC-cAMP and the response to cAMP (Fig. 4, A and B; and Fig. S11). In contrast to the WT spHCN channel, laser pulses applied in the presence of FITC-cAMP exerted minimal effects on the inactivation of the spHCN/H462 mutant channel and largely failed to initiate the transition of the channel from the inactivated state to the open state (Fig. 4 C). Laser pulses applied to the closed channel did have a moderate impact on the opening of the channel, reflected in moderate increase in I_{macro} (Figs. 4 D and S6). Compared with the WT channel, the extent of changes in the H462A mutant channel after photodynamic modification was much smaller (Fig. 4, E and F). Thus, for both spHCN and mHCN2 channels, the same conserved histidine residue in S6 appears to be critical for the photodynamic modification and the enhancement of the voltage-insensitive I_{inst} and I_{ss} components.

Application of Rose Bengal and $^1O_2$ quenchers/generator supports the involvement of $^1O_2$

To confirm that the above observations are the result of a photodynamic process, we chose Rose Bengal, a popularly used photosensitizer, in the absence of FITC-cAMP or regular cAMP. 100 nm Rose Bengal was applied to the bath solution in inside-out excised patch clamp experiments from cells expressing spHCN (Fig. 5 A). We found that laser pulses during the hyperpolarization voltage step triggered an increase in I_{macro}, I_{ss}, and I_{inst}, similar to our observation with FITC-cAMP in the bath solution (Fig. 5, B and D). When applied before voltage step to closed channels, laser pulses removed channel inactivation and introduced a prominent increase in I_{macro} (Fig. 5, C and E). In contrast, the spHCN/H462A mutant channel showed minimal responses to laser pulses with Rose Bengal in the bath, which is comparable to results with FITC-cAMP (Fig. S7).

To further confirm the involvement of $^1O_2$ in the photodynamic modification of spHCN channel, we tested whether $^1O_2$ quenchers, including sodium azide (1 mM) and Trolox-C (1 mM), would counteract the effect of laser light. In the presence of these $^1O_2$ quenchers, the effects of photodynamic modification were significantly diminished (Fig. 5 F, FITC-cAMP; Fig. 5 G, Rose Bengal; Fig. S8, Rose Bengal; laser pulses during voltage step; Fig. S9, Rose Bengal; laser pulse before voltage step). In addition, we tested the effects on Rose Bengal on membrane patches pulled from uninjected oocytes (i.e., not expressing spHCN). No obvious effects of laser light on the leak conductance were detected even with higher concentration of Rose Bengal (200 nM) and more laser pulses (up to 10; Fig. S10). Collectively, these results identify $^1O_2$ in photodynamic modification of spHCN channels.

Chemically generated $^1O_2$ modifies WT spHCN but not spHCN/H462A mutant channel

To further confirm the involvement of $^1O_2$ and exclude the involvement of other ROS, we tested the effect of H_2O_2 alone, ClO^- alone, or H_2O_2 together with ClO^-, a chemical reaction that has been widely used to generate $^1O_2$ (Fig. 6 A; Maetzke and Jensen, 2006; To et al., 2014). Separately applying H_2O_2 or ClO^- had no obvious effects on the function of spHCN channels; however, exposing the membrane patch to freshly mixed H_2O_2 and ClO^- produced an immediate increase in macroscopic current amplitude (Fig. 6, B and D). We noticed that the isolated membrane patch had to be mounted near the opening of the double-barrel glass pipette where H_2O_2 and ClO^- solutions flow out and mix (Fig. S12 A). This is consistent with the fact that $^1O_2$ has a very short lifetime (microseconds; Skovsen et al., 2005). Again, we repeated the same experiments on the spHCN/H462A mutant channel and observed no obvious responses to the chemical mixture of H_2O_2 and ClO^- (Fig. 6, C and D). Thus, for both WT and H462A mutant spHCN channels, chemically generated $^1O_2$ mimicked photodynamic modification but in the absence of light stimulation and photosensitizer.

Finally, we tested the sensitivity of the spHCN channel to hydroxyl radical and superoxide, the other two ROS (Fig. 6 E). We applied hydrogen peroxide and iron sulfate to the bath solution. After 6 min of incubation, no obvious changes in the function of the channel were apparent (Fig. 6 F). To test the involvement of superoxide, we added xanthine and xanthine oxidase to the bath solution (Fig. 6 G). Again, no obvious changes in the current traces were detected (Fig. S12, B and C). Notably, all chemicals were purchased fresh from vendors, but otherwise no positive controls were done to certify the chemical reactivity. In conjunction with the results of $^1O_2$ quenchers and generators, these observations support the involvement of $^1O_2$ in the photodynamic modification of spHCN channel and exclude the contribution from other ROS.

Discussion

Here we studied the photodynamic modification of spHCN channels by $^1O_2$, which had been generated through either canonical photodynamic processes or a chemical process in the absence of light. In the absence of cAMP, photodynamic modification of spHCN channels abolished the voltage-dependent channel inactivation and increased the hyperpolarization-activated I_h and the voltage-insensitive I_{inst}. These modification effects were mimicked by exposing spHCN channels to a chemical mixture of hypochlorite and hydrogen peroxide, which together with chemicals including $^1O_2$ quenchers or generators of other ROS helped establish $^1O_2$ as a critical player in the photodynamic modification of spHCN channels.

Remarkably, for both spHCN and mHCN2 channels, a highly conserved histidine residue located near the activation gate in S6 appears to be critical for the photodynamic modification. Both mHCN2/H434A and spHCN/H462A mutant channels show minimal responses to the light pulses applied during the hyperpolarization voltage command. For spHCN/H462A, light pulses applied to the channel in the closed state moderately increased current amplitude but largely failed to remove the inactivation of the channel. This difference between the WT and the H462A mutant channel should not be attributed to the binding of FITC-cAMP, as indicated by PCF measurements of binding (Fig. S11). Moreover, the spHCN/H462A mutant channel shows minimal responses to the $^1O_2$ generated through another photosensitizer (Rose Bengal) or through a chemical process (H_2O_2 + ClO^-). H462 in the spHCN channel could be the major substrate being modified by $^1O_2$. It is known that the imidazole ring in histidine reacts with $^1O_2$ at a very fast reaction rate ($5 \times 10^7\ M^{-1} \cdot s^{-1}$; Bisby et al., 1999; Méndez-Hurtado et al., 2012). The pair of electrons occupying the highest molecular orbital in $^1O_2$ show high reactivity toward electro-rich chemical structures, especially those with conjugated double bonds (Liu et al., 2014; Mano et al., 2014). It is possible that the $^1O_2$-histidine reaction involves the formation of endoperoxide as an intermediate and ends in a complex mixture of products, the mechanism of which is being investigated by both experimental and theoretical approaches (Méndez-Hurtado et al., 2012). Thus, further studies are needed to pinpoint the chemical nature of the reaction between $^1O_2$ and H462. Alternatively, it is possible that H462 is only one of several residues targeted by singlet oxygen. Other than histidine, residuals including tyrosine, methionine, cysteine, and tryptophan can also react with $^1O_2$ (Kim et al., 2008). Another explanation for the observations for spHCN/H462A mutant channel is that the histidine-to-alanine mutation limits the expression of I_{inst} and I_{ss}.

Previously, we had shown that the photodynamic modification of mHCN2 channels in the open state slows down channel deactivation and increases the component of I_{inst}, in contrast to the major effect on closed channels being the decrease in I_h (Gao et al., 2014). However, for spHCN channels, photodynamic modifications on both closed and inactivated channels abolish the channel inactivation. Photodynamic modification of closed spHCN channels leads to more pronounced increases in I_h but only a slight increase in I_{inst} and I_{ss}. These state-dependent responses to photodynamic modification by mHCN2 and spHCN could be attributed to subtle but critical structural reorganizations during the gating process that alter the accessibility of critical residues to $^1O_2$ at different conformations. For spHCN channels, its inactivation has been attributed to the reclosure of the same activation gate, caused by a loose coupling or slippage between the voltage sensor and the gate (Shin et al., 2004; Ryu and Yellen, 2012). Notably, H462 in spHCN and H434 in mHCN2 are located in the S6 and very close to the activation gate in both channels.

$^1O_2$ is one of the least understood ROS, partially because of its volatile chemical nature and the complex cross-interactions with signal transduction pathways (Sies et al., 2017). It is often difficult to pinpoint whether the contribution is truly mediated by $^1O_2$ but not by other ROS. Here, to confirm $^1O_2$ as the major player behind the photodynamic modifications, we applied a popular photosensitizer (Rose Bengal) and a chemical process to generate $^1O_2$ (hydrogen peroxide and hypochlorite), which produced comparable changes in channel behavior, especially in the removal of the channel inactivation of spHCN. The involvement of $^1O_2$ is further supported by the application of $^1O_2$ quenchers (sodium azide and Trolox-C), which effectively abolish the photodynamic modification effects. Moreover, we used a variety of chemicals to exclude the direct involvement of hydrogen peroxide, superoxide, and hydroxyl radicals. Importantly, all experiments were carried out on membrane patches without the interference from complex signaling pathways. Our study on the photodynamic modification of spHCN channels provides further insights into the modification of ion channels by $^1O_2$, a ubiquitous but still mysterious signaling molecule.

Acknowledgments

We acknowledge the technical support from C. Xie and T. Zhao. We are grateful to Dr. Sharona Gordon for her meticulous reading of the manuscript and to Dr. Lesley Anson for her help with the title and abstract.

This work was supported by National Institutes of Health grants R01GM098592 and R01GM109193 and startup funds from Virginia Commonwealth University to Q.L. and L.Z.

The authors declare no competing financial interests.

V. Idikuda, W. Gao, K. Grant, and Z. Su performed the experiments and analyzed the data. Q. Liu and L. Zhou analyzed the data and supervised the project. All chemical structures were downloaded from Wikipedia. All authors wrote the manuscript.

Kenton J. Swartz served as editor.

Submitted: 30 November 2017
Revised: 27 April 2018
Accepted: 15 June 2018

References

Agostinis, P., K. Berg, K.A. Cengel, T.H. Foster, A.W. Girotti, S.O. Gollnick, S.M. Hahn, M.R. Hamblin, A. Juzeniene, D. Kessel, et al. 2011. Photodynamic therapy of cancer: an update. *CA Cancer J. Clin.* 61:250–281. https://doi.org/10.3322/caac.20114

Babes, A., S.K. Sauer, L. Moparthi, T.I. Kichko, C. Neacsu, B. Namer, M. Filipovic, P.M. Zygmunt, P.W. Reeh, and M.J. Fischer. 2016. Photosensitization in porphyrias and photodynamic therapy involves TRPA1 and TRPV1. *J. Neurosci.* 36:5264–5278. https://doi.org/10.1523/JNEUROSCI.4268-15.2016

Baier, J., T. Maisch, M. Maier, E. Engel, M. Landthaler, and W. Bäumler. 2006. Singlet oxygen generation by UVA light exposure of endogenous photosensitizers. *Biophys. J.* 91:1452–1459. https://doi.org/10.1529/biophysj.106.082388

Barnes, S., and B. Hille. 1989. Ionic channels of the inner segment of tiger salamander cone photoreceptors. *J. Gen. Physiol.* 94:719–743. https://doi.org/10.1085/jgp.94.4.719

Bäumler, W., J. Regensburger, A. Knak, A. Felgenträger, and T. Maisch. 2012. UVA and endogenous photosensitizers—The detection of singlet oxygen by its luminescence. *Photochem. Photobiol. Sci.* 11:107–117. https://doi.org/10.1039/C1PP05142C

Biel, M., C. Wahl-Schott, S. Michalakis, and X. Zong. 2009. Hyperpolarization-activated cation channels: From genes to function. *Physiol. Rev.* 89:847–885. https://doi.org/10.1152/physrev.00029.2008

Bisby, R.H., C.G. Morgan, I. Hamblett, and A.A. Gorman. 1999. Quenching of singlet oxygen by Trolox C, ascorbate, and amino acids: Effects of pH and temperature. *J. Phys. Chem. A.* 103:7454–7459. https://doi.org/10.1021/jp990838c

BoSmith, R.E., I. Briggs, and N.C. Sturgess. 1993. Inhibitory actions of ZENECA ZD7288 on whole-cell hyperpolarization activated inward current (If) in guinea-pig dissociated sinoatrial node cells. *Br. J. Pharmacol.* 110:343–349. https://doi.org/10.1111/j.1476-5381.1993.tb13815.x

da Silva, E.F., F.M. Pimenta, B.W. Pedersen, F.H. Blaikie, G.N. Bosio, T. Breitenbach, M. Westberg, M. Bregnhøj, M. Etzerodt, L.G. Arnaut, and P.R. Ogilby. 2016. Intracellular singlet oxygen photosensitizers: on the road to solving the problems of sensitizer degradation, bleaching and relocalization. *Integr. Biol.* 8:177–193. https://doi.org/10.1039/C5IB00295H

DeRosa, M.C., and R.J. Crutchley. 2002. Photosensitized singlet oxygen and its applications. *Coord. Chem. Rev.* 233:351–371. https://doi.org/10.1016/S0010-8545(02)00034-6

Eisenman, L.N., H.J. Shu, G. Akk, C. Wang, B.D. Manion, G.J. Kress, A.S. Evers, J.H. Steinbach, D.F. Covey, C.F. Zorumski, and S. Mennerick. 2007. Anticonvulsant and anesthetic effects of a fluorescent neurosteroid analog activated by visible light. *Nat. Neurosci.* 10:523–530. https://doi.org/10.1038/nn1862

Fain, G.L., F.N. Quandt, B.L. Bastian, and H.M. Gerschenfeld. 1978. Contribution of a caesium-sensitive conductance increase to the rod photoresponse. *Nature.* 272:466–469. https://doi.org/10.1038/272467a0

Gao, W., Z. Su, Q. Liu, and L. Zhou. 2014. State-dependent and site-directed photodynamic transformation of HCN2 channel by singlet oxygen. *J. Gen. Physiol.* 143:633–644. https://doi.org/10.1085/jgp.201311112

Gauss, R., R. Seifert, and U.B. Kaupp. 1998. Molecular identification of a hyperpolarization-activated channel in sea urchin sperm. *Nature.* 393:583–587. https://doi.org/10.1038/31248

Jiang, H.N., Y. Li, and Z.J. Cui. 2017. Photodynamic physiology-photonanomanipulations in cellular physiology with protein photosensitizers. *Front. Physiol.* 8:191. https://doi.org/10.3389/fphys.2017.00191

Kanofsky, J.R., H. Hoogland, R. Wever, and S.J. Weiss. 1988. Singlet oxygen production by human eosinophils. *J. Biol. Chem.* 263:9692–9696.

Kim, J., M.E. Rodriguez, M. Guo, M.E. Kenney, N.L. Oleinick, and V.E. Anderson. 2008. Oxidative modification of cytochrome c by singlet oxygen. *Free Radic. Biol. Med.* 44:1700–1711. https://doi.org/10.1016/j.freeradbiomed.2007.12.031

Klotz, L.O., K.D. Kröncke, and H. Sies. 2003. Singlet oxygen-induced signaling effects in mammalian cells. *Photochem. Photobiol. Sci.* 2:88–94. https://doi.org/10.1039/B210750C

Kochevar, I.E. 2004. Singlet oxygen signaling: From intimate to global. *Sci. STKE.* 2004:pe7.

Liao, J.C., J. Roider, and D.G. Jay. 1994. Chromophore-assisted laser inactivation of proteins is mediated by the photogeneration of free radicals. *Proc. Natl. Acad. Sci. USA.* 91:2659–2663. https://doi.org/10.1073/pnas.91.7.2659

Liman, E.R., and L.B. Buck. 1994. A second subunit of the olfactory cyclic nucleotide-gated channel confers high sensitivity to cAMP. *Neuron.* 13:611–621. https://doi.org/10.1016/0896-6273(94)90029-9

Liu, F., W. Lu, Y. Fang, and J. Liu. 2014. Evolution of oxidation dynamics of histidine: Non-reactivity in the gas phase, peroxides in hydrated clusters, and pH dependence in solution. *Phys. Chem. Chem. Phys.* 16:22179–22191. https://doi.org/10.1039/C4CP03550J

Ludwig, A., X. Zong, M. Jeglitsch, F. Hofmann, and M. Biel. 1998. A family of hyperpolarization-activated mammalian cation channels. *Nature.* 393:587–591. https://doi.org/10.1038/31255

Macri, V., and E.A. Accili. 2004. Structural elements of instantaneous and slow gating in hyperpolarization-activated cyclic nucleotide-gated channels. *J. Biol. Chem.* 279:16832–16846. https://doi.org/10.1074/jbc.M400518200

Maetzke, A., and S.J.K. Jensen. 2006. Reaction paths for production of singlet oxygen from hydrogen peroxide and hypochlorite. *Chem. Phys. Lett.* 425:40–43. https://doi.org/10.1016/j.cplett.2006.04.097

Mano, C.M., F.M. Prado, J. Massari, G.E. Ronsein, G.R. Martinez, S. Miyamoto, J. Cadet, H. Sies, M.H. Medeiros, E.J. Bechara, and P. Di Mascio. 2014. Excited singlet molecular $O_2(^1\Delta g)$ is generated enzymatically from excited carbonyls in the dark. *Sci. Rep.* 4:5938. https://doi.org/10.1038/srep05938

Matheson, I.B., R.D. Etheridge, N.R. Kratowich, and J. Lee. 1975. The quenching of singlet oxygen by amino acids and proteins. *Photochem. Photobiol.* 21:165–171. https://doi.org/10.1111/j.1751-1097.1975.tb06647.x

Méndez-Hurtado, J., R. López, D. Suárez, and M.I. Menéndez. 2012. Theoretical study of the oxidation of histidine by singlet oxygen. *Chemistry.* 18:8437–8447. https://doi.org/10.1002/chem.201103680

Mistrík, P., A. Pfeifer, and M. Biel. 2006. The enhancement of HCN channel instantaneous current facilitated by slow deactivation is regulated by intracellular chloride concentration. *Pflugers Arch.* 452:718–727. https://doi.org/10.1007/s00424-006-0095-0

Ogilby, P.R. 2010. Singlet oxygen: There is indeed something new under the sun. *Chem. Soc. Rev.* 39:3181–3209. https://doi.org/10.1039/b926014p

Onyango, A.N. 2016. Endogenous generation of singlet oxygen and ozone in human and animal tissues: Mechanisms, biological significance, and influence of dietary components. *Oxid. Med. Cell. Longev.* 2016:2398573. https://doi.org/10.1155/2016/2398573

Prasad, A., U. Ferretti, M. Sedlářová, and P. Pospíšil. 2016. Singlet oxygen production in Chlamydomonas reinhardtii under heat stress. *Sci. Rep.* 6:20094. https://doi.org/10.1038/srep20094

Proenza, C., and G. Yellen. 2006. Distinct populations of HCN pacemaker channels produce voltage-dependent and voltage-independent currents. *J. Gen. Physiol.* 127:183–190. https://doi.org/10.1085/jgp.200509389

Proenza, C., D. Angoli, E. Agranovich, V. Macri, and E.A. Accili. 2002. Pacemaker channels produce an instantaneous current. *J. Biol. Chem.* 277:5101–5109. https://doi.org/10.1074/jbc.M106974200

Robinson, R.B., and S.A. Siegelbaum. 2003. Hyperpolarization-activated cation currents: From molecules to physiological function. *Annu. Rev. Physiol.* 65:453–480. https://doi.org/10.1146/annurev.physiol.65.092101.142734

Ryu, S., and G. Yellen. 2012. Charge movement in gating-locked HCN channels reveals weak coupling of voltage sensors and gate. *J. Gen. Physiol.* 140:469–479. https://doi.org/10.1085/jgp.201210850

Sack, J.T., N. Stephanopoulos, D.C. Austin, M.B. Francis, and J.S. Trimmer. 2013. Antibody-guided photoablation of voltage-gated potassium currents. *J. Gen. Physiol.* 142:315–324. https://doi.org/10.1085/jgp.201311023

Santoro, B., D.T. Liu, H. Yao, D. Bartsch, E.R. Kandel, S.A. Siegelbaum, and G.R. Tibbs. 1998. Identification of a gene encoding a hyperpolarization-activated pacemaker channel of brain. *Cell.* 93:717–729. https://doi.org/10.1016/S0092-8674(00)81434-8

Schneider, C.A., W.S. Rasband, and K.W. Eliceiri. 2012. NIH Image to ImageJ: 25 years of image analysis. *Nat. Methods.* 9:671–675. https://doi.org/10.1038/nmeth.2089

Schweitzer, C., and R. Schmidt. 2003. Physical mechanisms of generation and deactivation of singlet oxygen. *Chem. Rev.* 103:1685–1757. https://doi.org/10.1021/cr010371d

Shin, K.S., C. Maertens, C. Proenza, B.S. Rothberg, and G. Yellen. 2004. Inactivation in HCN channels results from reclosure of the activation gate: Desensitization to voltage. *Neuron.* 41:737–744. https://doi.org/10.1016/S0896-6273(04)00083-2

Sies, H., C. Berndt, and D.P. Jones. 2017. Oxidative stress. *Annu. Rev. Biochem.* 86:715–748. https://doi.org/10.1146/annurev-biochem-061516-045037

Skovsen, E., J.W. Snyder, J.D. Lambert, and P.R. Ogilby. 2005. Lifetime and diffusion of singlet oxygen in a cell. *J. Phys. Chem. B.* 109:8570–8573. https://doi.org/10.1021/jp051163i

Steinbeck, M.J., A.U. Khan, and M.J. Karnovsky. 1992. Intracellular singlet oxygen generation by phagocytosing neutrophils in response to particles coated with a chemical trap. *J. Biol. Chem.* 267:13425–13433.

To, T.L., M.J. Fadul, and X. Shu. 2014. Singlet oxygen triplet energy transfer-based imaging technology for mapping protein-protein proximity in intact cells. *Nat. Commun.* 5:4072. https://doi.org/10.1038/ncomms5072

Tour, O., R.M. Meijer, D.A. Zacharias, S.R. Adams, and R.Y. Tsien. 2003. Genetically targeted chromophore-assisted light inactivation. *Nat. Biotechnol.* 21:1505–1508. https://doi.org/10.1038/nbt914

Valenzeno, D.P., and M. Tarr. 1991. Membrane photomodification of cardiac myocytes: Potassium and leakage currents. *Photochem. Photobiol.* 53:195–201. https://doi.org/10.1111/j.1751-1097.1991.tb03923.x

Wojtovich, A.P., A.Y. Wei, T.A. Sherman, T.H. Foster, and K. Nehrke. 2016. Chromophore-assisted light inactivation of mitochondrial electron transport chain complex II in Caenorhabditis elegans. *Sci. Rep.* 6:29695. https://doi.org/10.1038/srep29695

Wu, S., Z.V. Vysotskaya, X. Xu, C. Xie, Q. Liu, and L. Zhou. 2011. State-dependent cAMP binding to functioning HCN channels studied by patch-clamp fluorometry. *Biophys. J.* 100:1226–1232. https://doi.org/10.1016/j.bpj.2011.01.034

Wu, S., W. Gao, C. Xie, X. Xu, C. Vorvis, F. Marni, A.R. Hackett, Q. Liu, and L. Zhou. 2012. Inner activation gate in S6 contributes to the state-dependent binding of cAMP in full-length HCN2 channel. *J. Gen. Physiol.* 140:29–39. https://doi.org/10.1085/jgp.201110749